buildings

MDPI

Article

A Numerical Investigation of the Influence of Diffuser Vane Height on Hydraulic Loss in the Volute for a Centrifugal Water Supply Pump

Zhen Liu [1], Xiangyuan Zhu [2,*], Jiying Liu [2], Moon Keun Kim [3] and Wei Jiang [4]

[1] Suzhou Architectural Decoration D&R Institute Co., Ltd., Suzhou 215021, China; sdm81927373@163.com
[2] School of Thermal Engineering, Shandong Jianzhu University, Jinan 250101, China; jxl83@sdjzu.edu.cn
[3] Department of Built Environment, Oslo Metropolitan University, N-0130 Oslo, Norway; moon.kim@oslomet.no
[4] College of Water Resources and Architectural Engineering, Northwest A&F University, Xianyang 712100, China; jiangweijt@nwafu.edu.cn
* Correspondence: zhuxiangyuan20@sdjzu.edu.cn

Abstract: The energy efficiency of water supply systems in high-rise residential buildings has become a significant concern for sustainable development in recent times. This work presents a numerical investigation on the influence of diffuser vane height on flow variation and hydraulic loss in the volute for a water supply centrifugal pump. Experiments and numerical simulations were conducted with four different vane height ratios. The numerical results were validated against experimental data. The hydraulic losses of different flow components were numerically evaluated at varying guide vane blade heights. The changes in flow patterns within the volute and the resulting discrepancies in hydraulic losses due to variations in the inlet flow conditions at different blade heights were studied. The findings indicate that the total pressure drop within the volute is affected significantly. Compared to traditional guide vanes, the reduced height vanes can reduce the hydraulic loss in the volute by nearly 75%. Once the vane height is reduced, the high-pressure gradient is improved, and the small-scale vortex vanishes. The influence area of the large-scale vortex in the volute outlet pipe decreases, leading to a weakening of the deflection of the main flow and ultimately resulting in reduced hydraulic loss.

Keywords: water supply pump; numerical simulations; hydraulic loss; vane height

Citation: Liu, Z.; Zhu, X.; Liu, J.; Kim, M.K.; Jiang, W. A Numerical Investigation of the Influence of Diffuser Vane Height on Hydraulic Loss in the Volute for a Centrifugal Water Supply Pump. *Buildings* **2024**, *14*, 2296. https://doi.org/10.3390/buildings14082296

Academic Editor: Alban Kuriqi

Received: 24 June 2024
Revised: 18 July 2024
Accepted: 23 July 2024
Published: 24 July 2024

1. Introduction

Building energy consumption is a significant contributor to overall energy usage, and enhancing the energy efficiency of building water supply systems presents an opportunity to optimize building energy utilization and decrease building carbon emissions [1,2]. Research suggests that the water supply system accounts for 1–4% of a building's electrical consumption and stands as the largest individual consumer of electricity within an entire city. The specific energy consumption of water supply systems ranges from 1.1 to 1.4 kWh/m^3 in certain Asian cities [3,4]. Approximately half of the energy loss in water supply systems is attributed to the pumping system [5]. Fluctuating water demand throughout the day often causes pumps to operate beyond their intended design parameters. This can trigger turbulent behavior within the pump, ultimately reducing system efficiency. Guide vanes can help enhance the intricate turbulent flow within the pump when it operates under off-design conditions [6].

The flow through a centrifugal pump with a vaned diffuser introduces complex flow distortion within the diffuser and volute, which is a focal point of pertinent research studies [7–10]. Within centrifugal pumps with vaned diffusers, rotating stall in partial load conditions is induced along with pressure fluctuations due to incorrect incidences of

the flow discharged by the impeller into the diffuser [8]. The backflow of fluid into the impeller channel predominantly occurs within the core flow zone and is more pronounced toward the suction side of the impeller blade in partial load conditions. This phenomenon is considered a potential source for the onset of diffuser stalling [9,11–14]. When rotating stall occurs in partial load conditions, the pressure fluctuation at the clearance between the impeller and diffuser displays a distinctive "starfish" shape. The radial force acting on the impeller's external wall at the liner ring section is comparable to that acting on the impeller blade and outer wall [12,15].

The presence of leading edge separations, high-frequency pressure fluctuations, radial forces, backflow, and rotating stall occurrences are common within centrifugal pumps equipped with vaned diffusers [15–17]. Hydraulic optimization of vaned diffusers is conducted to mitigate turbulence within pumps using methods such as response surface, multi-objective, and inverse design [18–20]. However, the presence of vanes isolating diffuser passages and factors like thick boundary layers at the diffuser inlet or non-uniform velocity distributions, such as those caused by an upstream bend, can lead to deteriorated pressure recovery and an increased risk of separation, potentially resulting in rotating stall occurrences. The presence of rotating stall, backflow, and pressure fluctuations is consistently observed [21,22]. The reduced vane height diffuser first utilized in turbomachinery can balance flow non-uniformity among different guide vane passages, creating a more uniform circumferential flow and enhancing pressure recovery performance for centrifugal pumps. This, in turn, reduces alternating stress on the impeller, thereby improving its overall performance [23]. This highlights the potential benefits of utilizing reduced vane height diffusers in turbomachinery applications. Building upon the findings regarding reduced vane height diffusers in turbomachinery, the authors of the previous work applied reduced vane height diffusers to centrifugal pumps [24,25]. This application likely aimed to leverage the benefits observed in turbomachinery systems and adapt them to enhance the performance of centrifugal pumps.

The findings show that the pump with reduced height diffuser vanes obtains higher efficiency compared to vaneless diffusers and a wider high-efficiency operating range compared to vaned diffusers. And the radial force on the impeller is also significantly enhanced. However, the effects of reduced vane height on flow characteristics and total pressure loss remain uncertain. The present work aims to examine the impact of diffuser vane height on the internal flow characteristics in a centrifugal pump. The evaluation commences by assessing the total pressure loss in each flow component. Subsequently, starting from the inlet conditions, the present study investigates how vane height affects the flow characteristics of the overflow components. The dependency of total pressure loss on the flow characteristics is investigated. This study seeks to provide insights into optimizing water supply centrifugal pump performance through diffuser design considerations. The flowchart of the research methodology is described in Figure 1.

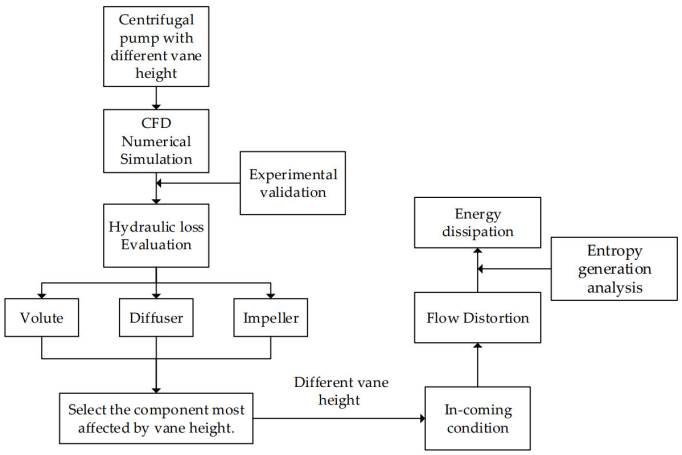

Figure 1. Flowchart of research methodology.

2. Numerical Setup and Validation

2.1. Parameters and Mesh Refinement

The design parameters of the centrifugal pump with specific speed (n_s) of 55 are displayed in Table 1. Figure 2 illustrates a schematic illustration of the vaned diffuser. To analyze the effect of diffuser vane height on the internal flow characteristics of the centrifugal pump, the relative vane height h/b is adjusted to values of 1, 0.8, 0.6, and 0.4. Here, b denotes the width of the diffuser outlet, and h signifies the vane height. Consequently, the flow passage of the diffuser is divided into the vaned region and the vaneless region.

Table 1. Design parameters of the centrifugal pump.

Flow Rate Q_{des} (m^3/s)	Head H_{des} (m)	Blade Number Z_b	Vane Number Z_v	Rotational Speed n (rpm)
1.11×10^{-2}	55	6	5	2900

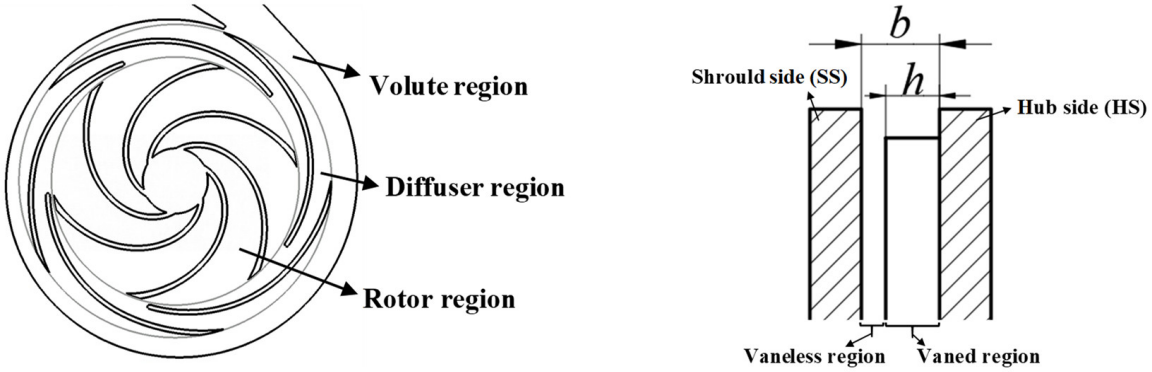

(**a**) A schematic illustration of the pump (**b**) A schematic illustration of the vaned diffuser

Figure 2. A schematic illustration of the vaned diffuser.

Structured grids are used to discretize the computational domain with Ansys ICEM-CFD v 10.0, incorporating additional mesh refinement at the boundaries, as depicted in Figure 3. The sst k-ω turbulence model is employed for turbulence prediction. The pressure inlet and mass flow outlet are set for the boundaries. The pressure inlet and mass flow outlet boundary conditions are specified. The time-step size is determined as the time taken for the impeller to rotate by 1°, which is set to 5.7471264×10^{-5} s. The grid convergence analysis was conducted by comparing the head coefficients obtained from different mesh configurations at different flow rates, as shown in Figure 4. The numerical calculations were carried out at $h/b = 1$. The head coefficient is evaluated as

$$\phi = \frac{gH}{0.5u_2^2} \tag{1}$$

where u_2 stands for the speed of the impeller outlet; H denotes the head.

Given that the flow within a centrifugal pump is incompressible, the governing equations for it are as follows:

$$\frac{\partial u_i}{\partial x} = 0 \tag{2}$$

$$\frac{\partial u_i}{\partial t} + u_j \frac{\partial u_i}{\partial x_j} = -\frac{1}{\rho}\frac{\partial p}{\partial x_i} + \nu \frac{\partial^2 u_i}{\partial x_j \partial x_j} + S_i \tag{3}$$

where u_i stands for the velocity component; S_i denotes the source term.

Under partial load conditions, there is a noticeable difference in the head between G1 and the other three cases. This difference diminishes as the number of grids increases and becomes negligible when the grid number exceeds G2. The maximum relative difference in head coefficients between the G2 and G4 meshes is less than 2%. Therefore, the G2 mesh has been selected for further numerical research. Additionally, the y plus values across the domain at the design flow rate are depicted in Figure 4. The illustration shows that the y plus values across the domain are below 110, indicating accuracy in predicting near-wall flow behavior.

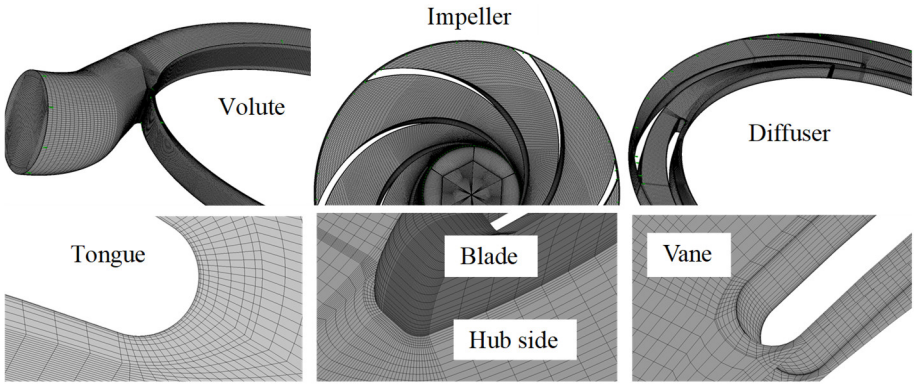

Figure 3. A schematic illustration of the discretized domain.

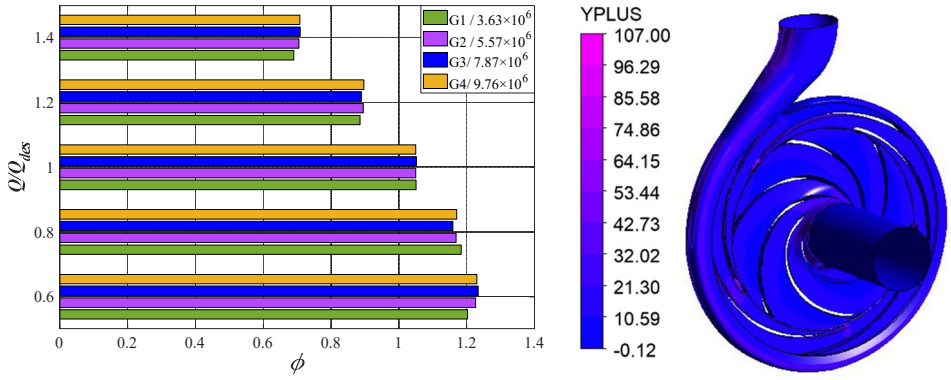

(**a**) Head coefficient Φ at different flow rates (**b**) y plus at design flow rate

Figure 4. Mesh convergence study and y plus at design flow rate.

2.2. Experimental Analysis and Numerical Methods Validation

In the test, two types of sensors were used, absolute pressure sensors with measuring range of 0–0.12 MPa and gauge pressure sensors with measuring range of 0–0.5 MPa. The output voltage signal for these sensors ranges from 0 to 5 V. The uncertainty of the pressure measurement is assessed according to Ref. [26], which is shown in Table 2. It is demonstrated that the uncertainty of the pressure measurement is less than 0.9%.

Table 2. Uncertainty involve with pressure measurement.

	Abxolute Pressure Sensor	**Gague Pressure Sensor**
Measurement location	Pump inlet	Other pressure probe
Minimum value/MPa	0.0922	0.0934
Uncertainty/%	0.3421	0.8293

The test rig and validation of the numerical heat coefficient through experimentation with h/b = 1 are depicted in Figure 5. Pressure probes P1 and P2 are located at the tongue

and downstream of the tongue. While the difference between the numerical and experimental head coefficient curves is more pronounced in overload conditions compared to partial load conditions, the trend of the head increasing with the flow rate in the numerical simulations mirrors that observed in the experiments as the flow rate increases. Additionally, the numerical head consistently exceeds the experimental value by less than 5% across different operating flow rates. Based on these findings, the numerical simulations can be considered reliable for predicting the fluid dynamics within the pump.

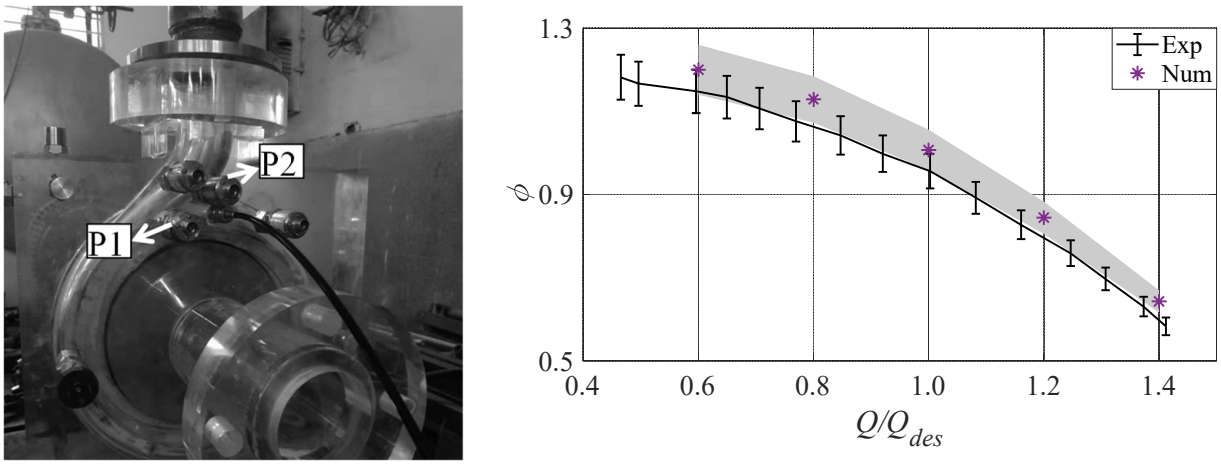

Figure 5. Test rig and numerical simulation validation.

Figure 6 shows the head coefficient obtained in the experiments with different vane heights. The present study demonstrates that as the diffuser vane height decreases, the head increases under overload conditions, as does the efficiency, while they decrease under partial load conditions. This highlights the significant impact of vane height on the head and efficiency, indicating that vane height plays a substantial role in influencing fluid flow within the pump.

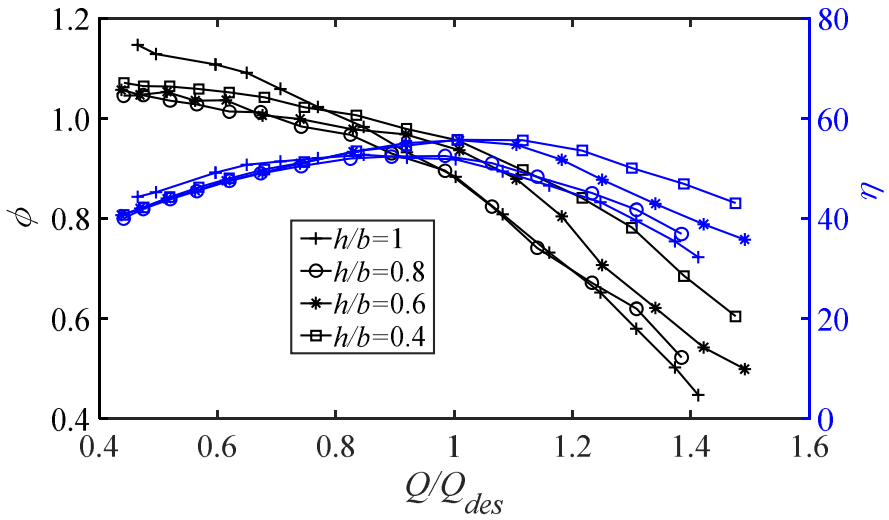

Figure 6. Head coefficient in experiments.

Figure 7 illustrates the pressure coefficient in the frequency domain, as well as the time-history value and the amplitude of the pressure coefficient at the dominant frequency at probes P1 and P2 for various vane heights across different flow rates. The data indicate that the guide vane height notably influences pressure fluctuations near the tongue. Specifically, the amplitude of pressure fluctuations at the dominant frequency is significantly higher

when the vane height ratio (h/b) is 1 compared to other vane heights. This difference in amplitude with different vane heights is most pronounced at P2. The amplitude is reduced to approximately 70% for P1 and 80% for P2 at the design flow rate as the vane height ratio (h/b) decreases from 1 to 0.6. Nevertheless, it is important to note that the amplitude does not decrease monotonically with decreasing vane height. The amplitude sharply decreases when the vane height reduces from h/b = 1 to h/b = 0.6, and then decreases smoothly from h/b = 0.8 to h/b = 0.6, reaching its minimum value. Subsequently, as the blade height further decreases from h/b = 0.6, the amplitude begins to increase. The dominant frequency, known as the blade-passing frequency, is induced by impeller–tongue interactions. The findings suggest that vane height has a significant influence on rotor–stator interactions and the flow field around the tongue.

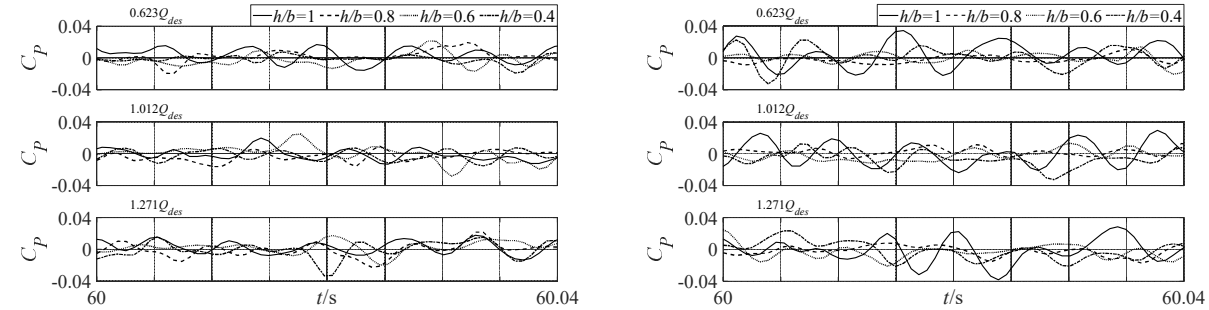

(**a**) Pressure coefficient at probes P1 and P2

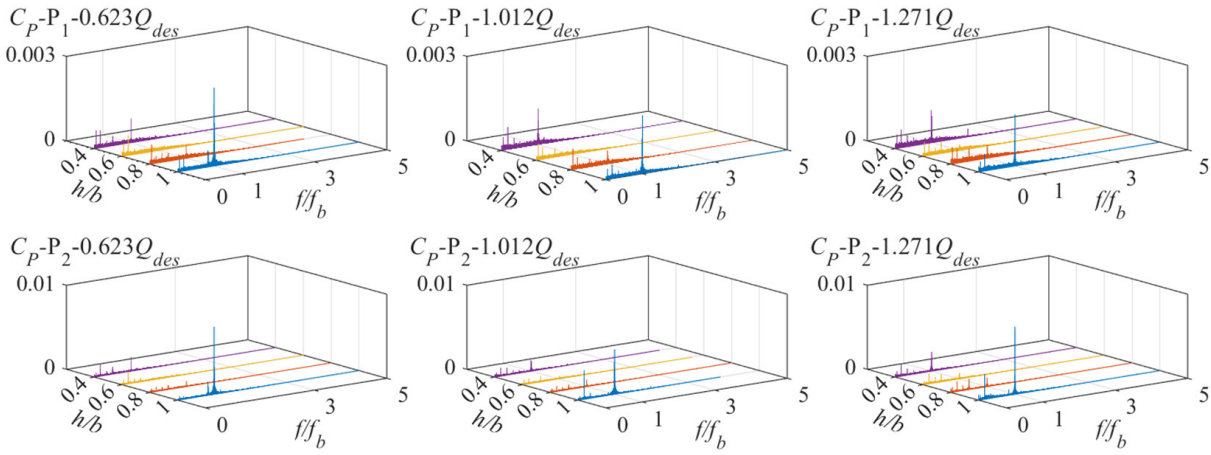

(**b**) Frequency domain of pressure coefficient at P1 and P2

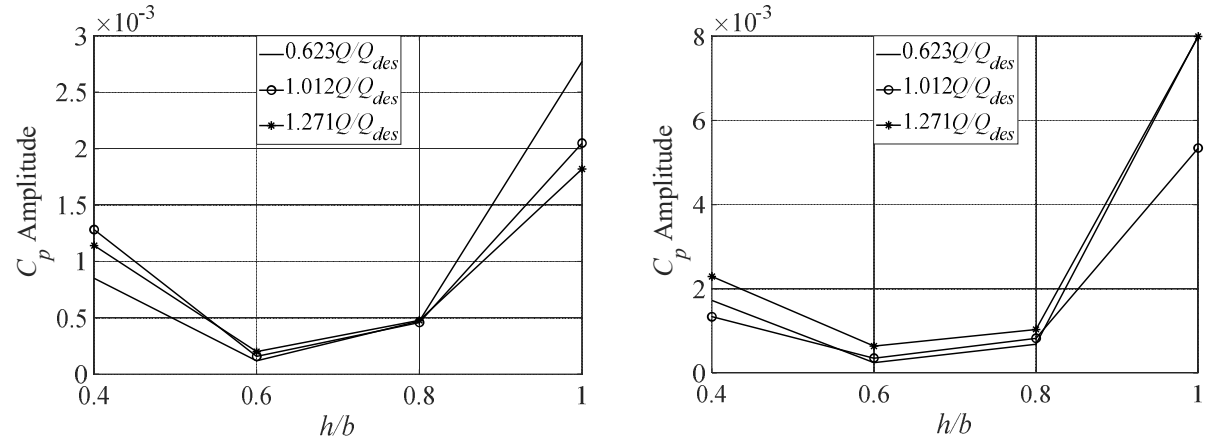

(**c**) Amplitude of pressure coefficient at dominant frequency for P1 and P2

Figure 7. The pressure coefficient and its frequency domain at probes P1 and P2.

To assess the strength of pressure fluctuations, the standard deviation is evaluated as shown in Figure 8. It is demonstrated that the strength of pressure fluctuations is clearly influenced by vane height, particularly at P2. The strength of pressure fluctuations is reduced to approximately 20% for P1 and 40% for P2 at the design flow rate as the vane height ratio (h/b) decreases from 1 to 0.6. When considering P1, reducing the blade height can mitigate the intensity of pressure fluctuations, as observed with h/b = 0.8 or h/b = 0.6. However, excessively reducing the blade height may lead to increased pressure fluctuation intensity at design and high flow rates, as evidenced by h/b = 0.4 under high-flow conditions. This phenomenon can be attributed to the pressure probe's location on the shroud side, where the diffuser is vaned, as depicted in Figure 2. Decreasing the vane height results in interference between flow fields in the vaned and vaneless regions, leading to more pronounced fluctuations in the vaned region. As the probe P2 moves downstream of the tongue, the interference effect diminishes, and reducing the vane height can notably decrease the intensity of pressure fluctuations, as illustrated in Figure 8.

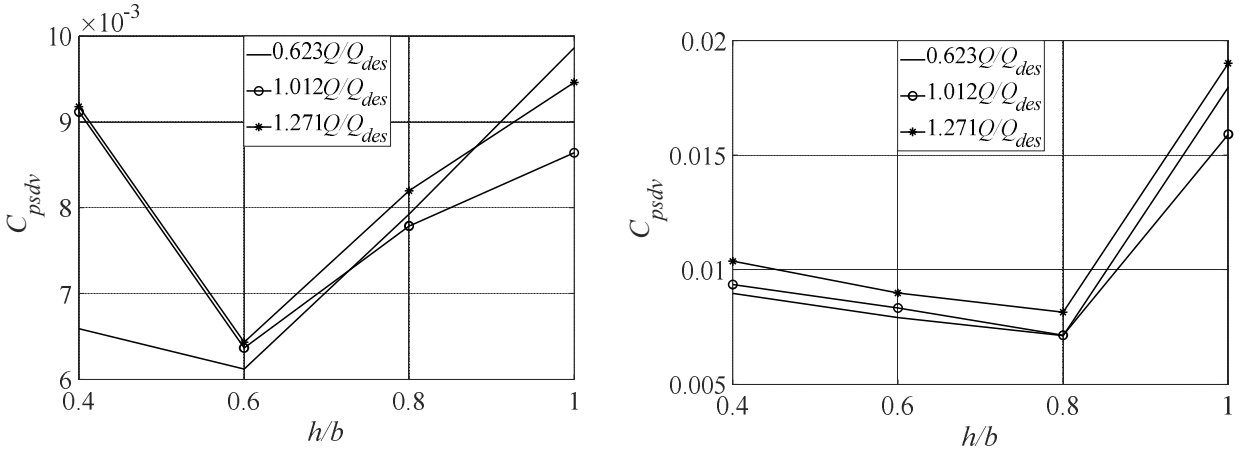

Figure 8. The standard deviation of pressure fluctuations for P1 and P2.

3. Results and Discussion

To assess energy conversion in each component and further investigate the impact of vane height on flow structure, Figure 9 illustrates the total pressure drop in each component. The non-dimensionalized total pressure drop and work conducted by the impeller is evaluated as follows:

$$\phi_{\text{suffix}} = \frac{P_p - P_s}{0.5\rho u_2^2} \tag{4}$$

$$W_{sft} = \frac{\frac{2\pi * Mn}{60}}{u_2 * A_2 * 0.5 * \rho * u_2^2} \tag{5}$$

where ϕ_{suffix} represents the total pressure drop, and suffix represents d (diffuser), r (rotor), and w (volute); P_p and P_s represent the total pressure at the pressure side and the suction side of the component, respectively; W_{sft} stands for the shaft power, and M, n, and A_2 represent the torque, rotation speed, and area of the impeller outlet, respectively.

The shaft power demonstrates minimal variation at different vane heights across all flow rates, with the maximum difference not exceeding 2.5%. Additionally, the total pressure drop within the impeller also exhibits minimal variation at different vane heights across all flow rates, with the maximum difference not exceeding 1%. This suggests that vane height has little influence on the time-averaged flow field within the impeller. The total pressure drop in the diffuser and volute presents significant differences at different vane heights, especially in overload conditions. The total pressure drop within the diffuser for an h/b less than 1 increases as the flow rate increases. However, at h/b = 1, it decreases to its minimum at the design flow rate and then increases with further increases in flow rate. Besides the total pressure drop decreases with vane height decreases, the difference in

the total pressure drop at 0.6 Q/Q_{des} is smaller compared to other flow rates. At 1.4 Q/Q_{des}, the difference in the total pressure drop between the guide vanes with h/b = 0.4 and h/b = 1 is approximately 35%.

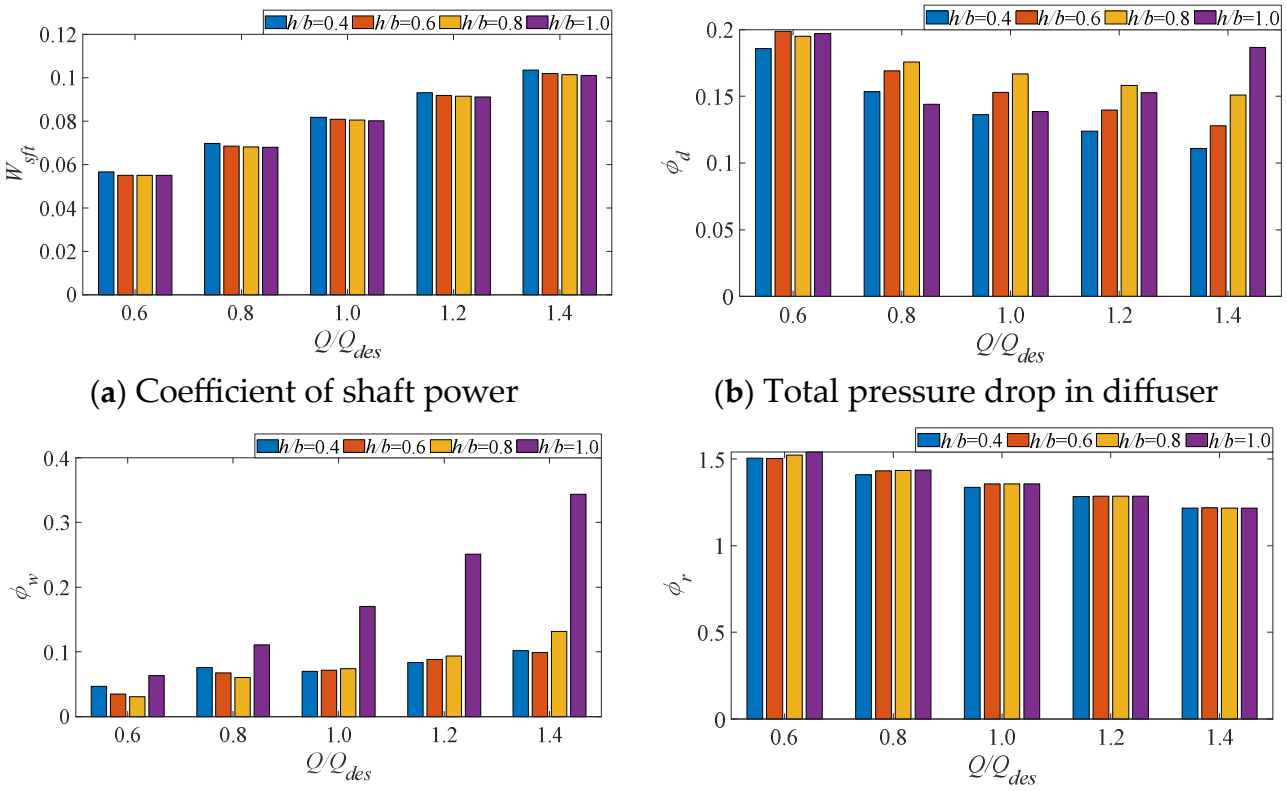

Figure 9. Total pressure drop in each component.

The total pressure drop in the volute increases as the flow rate increases. At 1.4 Q/Q_{des}, the difference in the total pressure drop in the volute between the guide vanes with h/b = 0.4 and h/b = 1 is approximately 75%. The total pressure drop in the static component presents hydraulic loss. As the vane height decreases, clearance between the vane and hub exists, leading to varying hydraulic losses in the diffuser due to complex clearance flow. However, it is worth noting that the hydraulic loss in the volute varies significantly due to different diffuser vane heights, indicating that the diffuser vane height has a significant influence on the flow field in the volute.

Figure 10 illustrates the time-averaged pressure at the volute inlet for different vane heights at three flow rates. It is illustrated that the pressure decreases roughly in the direction of rotation away from the tongue and reaches its minimum value at θ_r = 330°. At 0.8 Q/Q_{des}, the pressure decreases more sharply with h/b = 1 than with an h/b less than 1, and the variance is reduced with increasing flow rate. It is important to note that with h/b = 1, the pressure varies sharply around the tongue and changes to be more smooth when the h/b is less than 1. This suggests that the pressure distribution is more uniform with an h/b less than 1 than with h/b = 1.

The transient radial velocity (v_r) distribution at the volute inlet (the turning surface in Figure 10) for various time steps and diffuser vane heights is illustrated in Figure 11, with the white line representing the vane trailing edge. The radial velocity exhibits minimal changes over time, with the most noticeable differences observed near the tongue, as indicated by the square marker in Figure 11a. However, it is evident that the radial velocity shows significant differences with varying vane heights, particularly in the tongue region, as indicated by the square marker in Figure 11b. It is demonstrated that when h/b = 1, the

radial velocity at diffuser passages far away from the tongue shows minimal differences, as illustrated by the dashed square marker. In contrast, the radial velocity at passages near the tongue exhibits significant differences compared to other passages. When the h/b is less than 1, the difference between diffuser passages decreases, but the passage upstream of the tongue presents distinct differences compared to others.

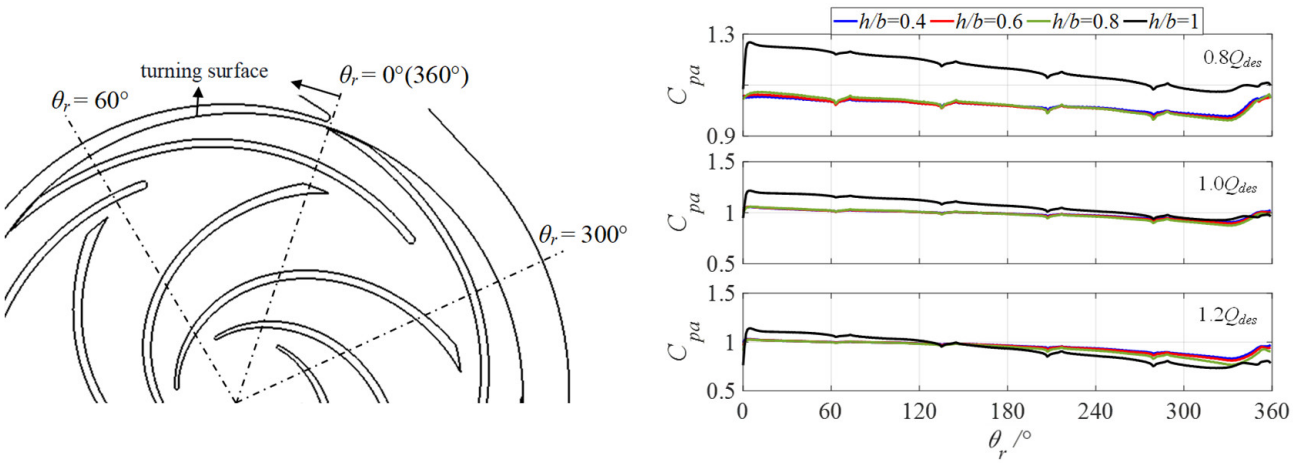

Figure 10. Time-averaged pressure at volute inlet.

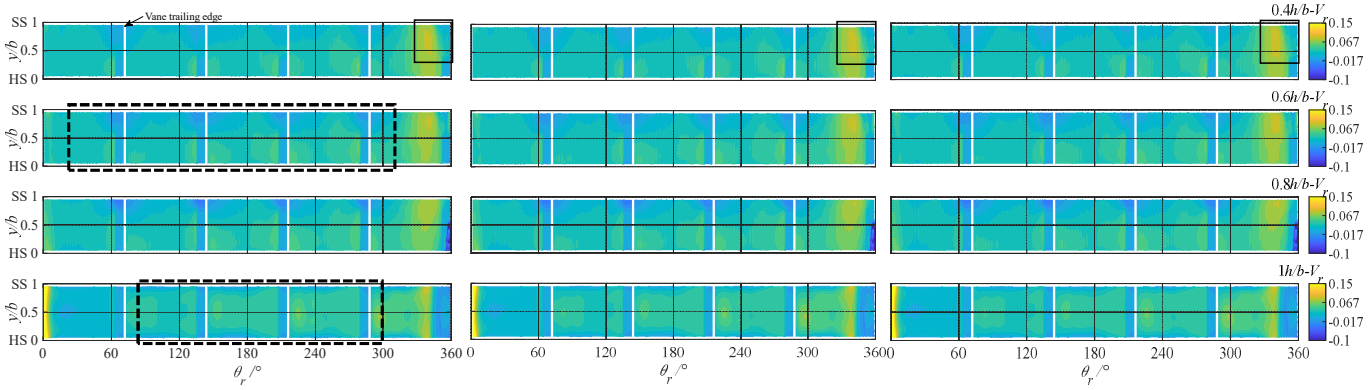

(**a**) 0.8 Q/Q_{des}

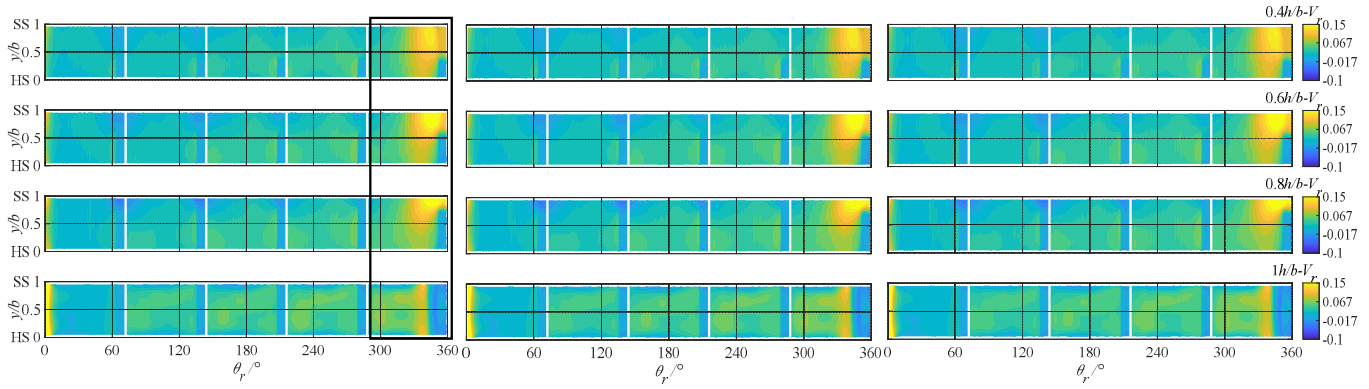

(**b**) 1.0 Q/Q_{des}

Figure 11. *Cont.*

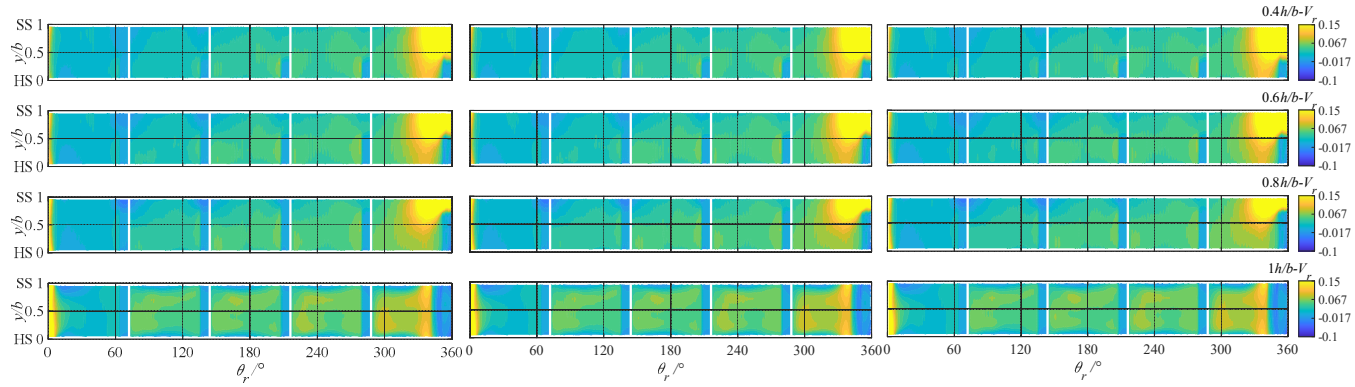

(**c**) 1.2 Q/Q_{des}

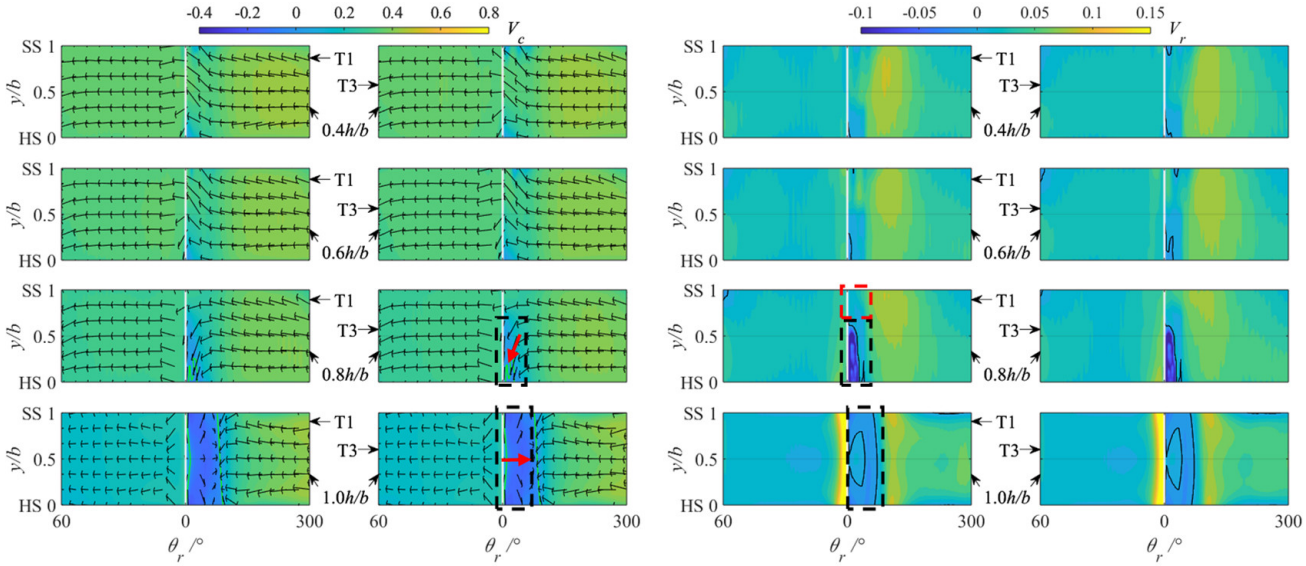

(**d**) 0.8 Q/Q_{des}

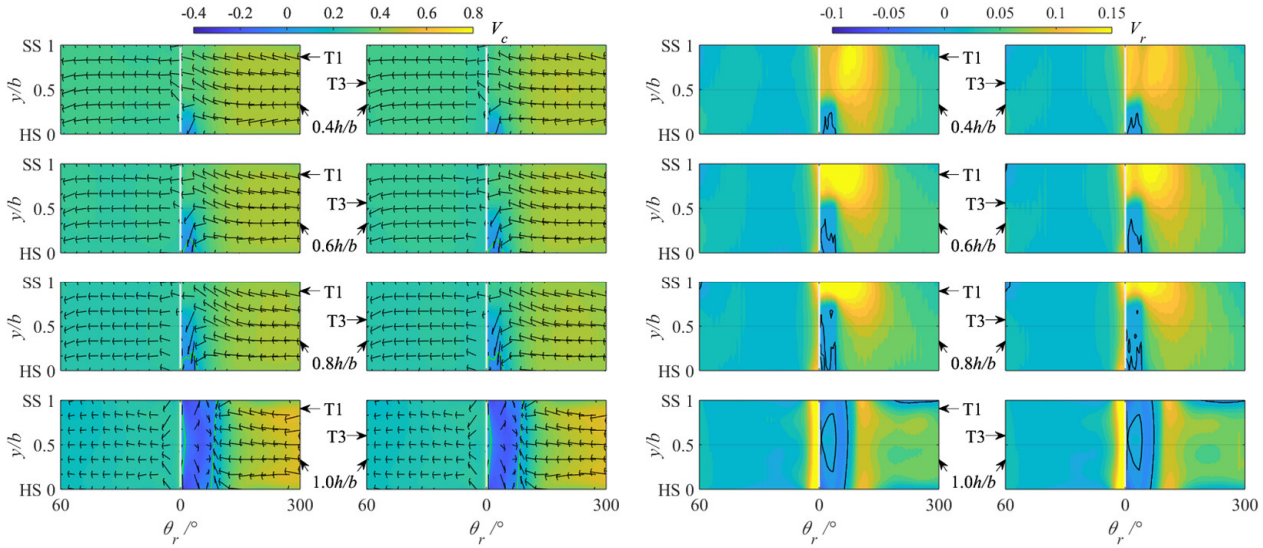

(**e**) 1.0 Q/Q_{des}

Figure 11. *Cont.*

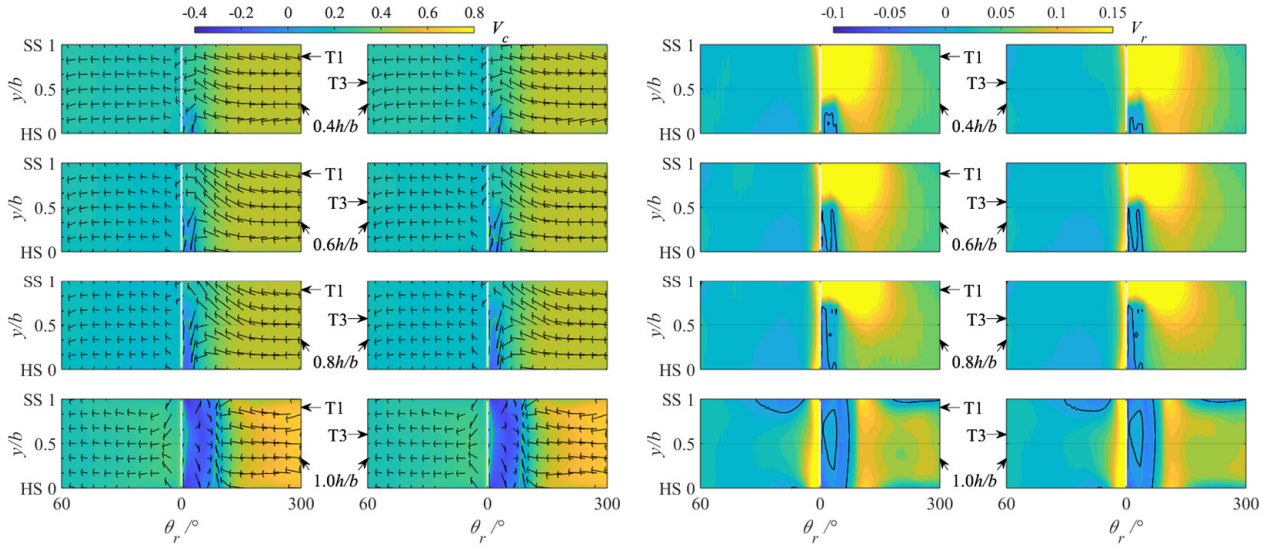

(**f**) 1.2 Q/Q_{des}

Figure 11. Radial velocity at volute inlet under different time steps for different vane heights.

To facilitate a more intuitive display and analysis of the variances in the tongue area for various guide vane heights, Figure 11d–f illustrate the distributions of circumferential (v_c) and radial velocities around the tongue. As previously stated, the variations in velocity over time are significantly smaller compared to the changes observed with blade height. Regardless of the flow rate, the trend in the impact of blade height on the flow at the tongue area remains consistent. As the flow rate increases, both the radial velocity and the circumferential velocity also increase, while the distribution of these velocities remains similar across different flow rates.

As shown in Figure 11d, a reverse flow region marked by a dashed square and a red arrow exists in front of the tongue for the vaned diffuser with a vane height ratio of 1 ($h/b = 1$), where the radial velocity alternates between positive and negative values. The radial velocities on both the upstream and downstream sides of the reverse flow region are significant. These observations can be attributed to a high-pressure gradient caused by a blocking effect from the tongue, as illustrated in Figure 10. As the vane height decreases to $h/b = 0.8$, the reverse flow region vanishes and the negative radial velocity region becomes smaller. The direction of the circumferential velocity is deflected toward the hub side, where, similar to a sink, the radial velocity is negative. It is notable that this region is vaned. In the vaneless area, the circumferential velocity exhibits more uniformity, particularly at high flow rates. Additionally, the circumferential and radial velocity in the vaneless region is noticeably larger. When the vane height is further reduced, the negative radial velocity region continuously decreases and may even disappear at lower flow rates. As the flow rate increases, these observations become more prominent. Nevertheless, even with a reduced vane height, the negative radial velocity region persists under overload conditions, although it may occupy a smaller area. Reducing the vane height has been shown to decrease the blocking effect caused by the tongue. It is readily apparent that this reduction in vane height can help alleviate or lessen the interference or obstruction typically caused by the tongue.

Figure 9c demonstrates that the total pressure drop in the volute is significantly influenced by the vane height. The fluid discharged from the diffuser flows over the tongue and then into the volute outlet pipe. The flow field in the tongue region is sensitive to the vane height and notably differs from the region far away from the tongue, as demonstrated in Figure 11. Considering the radial and circumferential velocity variations with vane height, the flow field in the volute is expected to change significantly with diffuser vane

height, leading to different hydraulic losses in the outlet pipe. Figure 12 displays the streamlines on the midsection for different vane heights at 1.2 Q_{des}. It is evident that with a vane height ratio of h/b = 1, a small clearance between the tongue and the vane trailing edge is formed, where a very high-pressure gradient is observed, as illustrated in Figure 10, resulting in a small vortex in front of the tongue, as shown in Figure 12c. The reverse flow and negative radial velocity are induced, as depicted in Figure 11. Additionally, a large-scale vortex at the outlet pipe, marked with a dashed line arrow, contributes to a squeezing effect on the main flow, while the small-scale vortex enhances this effect, causing deflection of the main flow away from the tongue, as indicated by the blue arrows. For vane height ratios h/b less than 1, the pressure gradient is significantly reduced due to the presence of the vaneless region. The small-scale vortex disappears, and the strength and influence area of the large-scale vortex at the outlet pipe decrease. The reverse flow and negative velocity region also decrease, leading to an improvement in the deflection of the main flow. The variation in hydraulic loss with vane height can be attributed to these changes in the flow field.

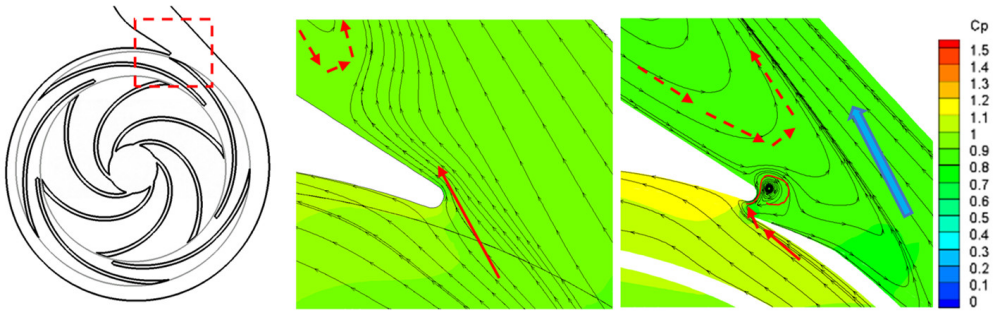

(**a**) Location (**b**) h/b = 0.4 (**c**) h/b = 1.0

Figure 12. Streamline on midsection for different vane heights at 1.2 Q_{des}.

To assess the variation in hydraulic loss with vane height, an entropy generation analysis method with Computational Fluid Dynamics (CFD) is adopted. Based on research findings [27,28], the energy loss can be categorized into viscous loss and turbulent loss. The former is influenced by the time-averaged velocity gradient, while the latter is attributed to fluctuating velocity. Therefore, the energy loss can be quantified using Equations (4)–(6).

$$\psi = \overline{\psi} + \psi' \tag{6}$$

$$\overline{\psi} = \mu[2(\frac{\partial \overline{V_i}}{\partial x_i})^2 + (\frac{\partial \overline{V_i}}{\partial x_j} + \frac{\partial \overline{V_j}}{\partial x_i})^2] \tag{7}$$

$$\psi' = \rho(\nu \overline{\frac{\partial V'_i}{\partial x_k} \frac{\partial V'_i}{\partial x_k}} + \nu \frac{\partial^2 \overline{V'_i V'_j}}{\partial x_i \partial x_j}) \tag{8}$$

where V stands for velocity.

Given that the second term on the right-hand side of Equation (7) is consistently smaller, particularly in high-Reynolds-number regions, the turbulent energy loss is approximated by the first term. Subsequently, the turbulent loss component can be determined using the kinetic energy dissipation, as expressed in Equation (9).

$$\psi' = \rho\varepsilon \tag{9}$$

Figure 13 illustrates the hydraulic loss in the mid-cross-section of the volute for various vane heights at 1.2 Q/Q_{des}. It is evident that hydraulic loss primarily occurs at the outlet pipe of the volute. The hydraulic loss is notably higher with a vane height ratio h/b of 1.0 compared to h/b = 0.6. In the case of h/b = 1.0, the hydraulic loss arises in areas where

the main flow and interactions with large-scale vortices occur, indicating a significant velocity gradient. As $h/b = 0.6$, the influence area of large-scale vortex decreases, resulting in improved main flow deflection and a reduced fluid flow gradient, ultimately leading to decreased hydraulic loss.

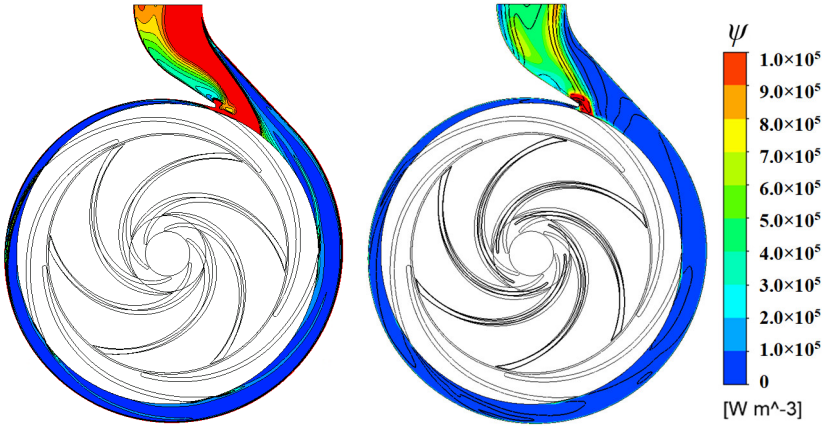

Figure 13. Hydraulic loss at volute mid-section at 1.2 Q/Q_{des}.

Figure 14 displays the hydraulic loss in three cross-sections of the outlet pipe under varying vane heights and operating conditions. Additionally, streamlines and velocity contour lines are depicted. The visualization indicates that hydraulic loss occurs in regions with a high velocity and more intense contour lines. As the diffuser vane height decreases, the deflection of the main flow becomes more uniform, leading to a reduced velocity and gradient, thereby improving hydraulic loss. In the area marked with a circular line, locally higher hydraulic loss is observed, likely due to being downstream of the vaneless region of the diffuser outlet where the velocity and gradient are relatively high.

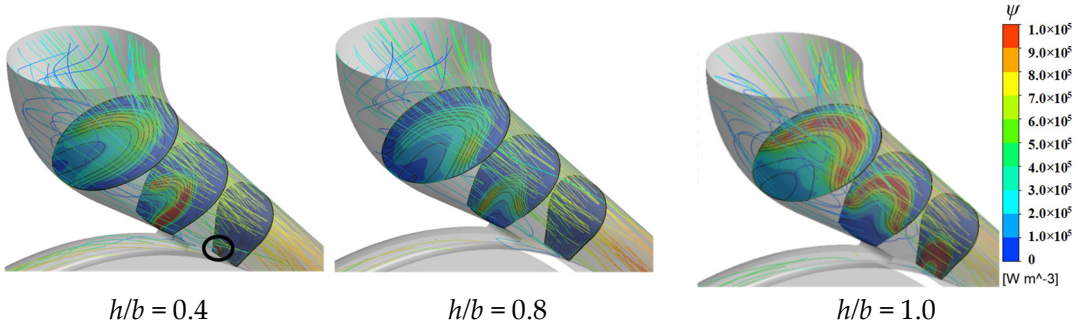

(**a**) Hydraulic loss at volute cross-section at 0.8 Q/Q_{des}

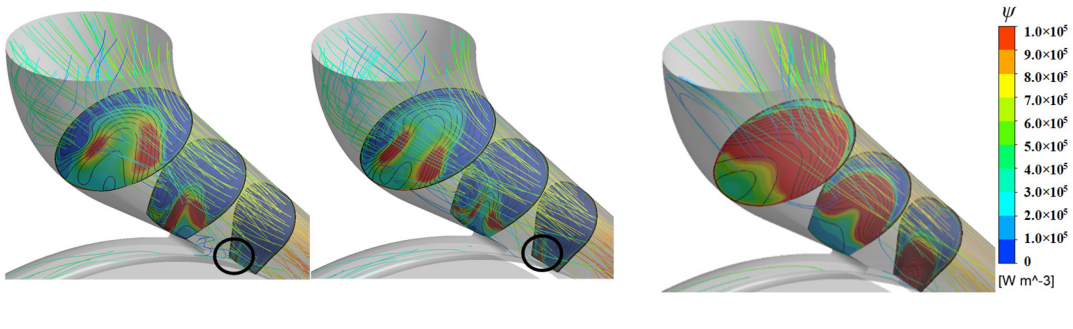

(**b**) Hydraulic loss at volute cross-section at 1.2 Q/Q_{des}

Figure 14. Hydraulic loss at volute cross-section for different vane heights and flow rates.

4. Conclusions

The current study showcases the impact of vane height on energy loss in the volute of a centrifugal pump. Experimental assessments are conducted to evaluate pressure fluctuations at the tongue and downstream of the tongue. The total pressure loss in various flow components for varying vane heights is analyzed. Subsequently, the flow pattern at the volute inlet and hydraulic loss within the volute are investigated using visualized methods.

Reducing the diffuser vane height leads to a significant decrease in pressure fluctuation intensity and amplitude at the dominant frequency at the tongue and downstream of the tongue. While the diffuser vane height has a minimal impact on the time-averaged shaft power of the centrifugal pump impeller, it has a notable effect on hydraulic loss in the volute. With an increasing flow rate, the reduction in hydraulic loss becomes more pronounced with a decreased vane height.

The reduced height vane leads to a more uniform pressure distribution at the volute inlet along the circumferential direction, eliminating the high-pressure gradient phenomenon at the tongue. This results in the disappearance of recirculation vortices at the tongue observed with traditional guide vanes, along with the elimination of regions of negative radial velocity and reverse flow at the tongue. Consequently, the blocking effect of the vortices at the tongue and outlet pipe of the volute is eliminated, leading to an improvement in the deflection of the main flow in the outlet pipe of the volute and a decrease in the hydraulic loss caused by the relatively high velocity and its gradient induced by flow deflection. This indicates that the reduced height guide vanes can effectively enhance pump efficiency and reduce energy consumption over a broad range of flow rates, playing a positive role in energy saving for building water supply systems.

Although reduced height guide vanes can enhance pump performance, particularly by significantly reducing the energy loss in the volute, the energy loss of the guide vanes themselves is unknown with variations in vane height, and the optimal blade height requires additional investigation, which will be the subject of subsequent research.

Author Contributions: Conceptualization, Z.L., X.Z. and J.L.; Methodology, X.Z. and J.L.; Software, W.J.; Validation, Z.L.; Formal analysis, Z.L. and X.Z.; Data curation, M.K.K.; Writing—original draft, Z.L.; Writing—review & editing, X.Z., J.L., M.K.K. and W.J.; Funding acquisition, X.Z. All authors have read and agreed to the published version of the manuscript.

Funding: This research was funded by Natural Science Foundation of Shan Dong Province (grant no. ZR2021QE258), Science and Technology-based Enterprises Innovation Capacity Enhancement Project (grant no.2023TSGC0979), Doctoral Foundation of Shandong Jianzhu University (grant no. X21014Z).

Data Availability Statement: The original contributions presented in the study are included in the article, further inquiries can be directed to the corresponding authors.

Conflicts of Interest: Author Zhen Liu was employed by the company Suzhou Architectural Decoration D&R Institute Co., Ltd. The remaining authors declare that the research was conducted in the absence of any commercial or financial relationships that could be construed as a potential conflict of interest.

Nomenclature

A_2	area of impeller outlet, m^2
C_p	pressure coefficient
C_{PSDV}	standard deviation of pressure
H	head, m
H_{des}	head at design flow rate, m
M	torque, N·m
P	pressure, Pa
P_P	pressure at pressure side, Pa
P_S	pressure at suction side, Pa
Q	volume flow rate, m^3/h

Q_{des}	volume flow rate at design point, m^3/h
ϕ	head coefficient
ρ	density, kg/m^3
θ_r	angular coordinate, °
υ	dynamic viscosity, Pa·s
b	vane height, mm
g	gravitational acceleration, m/s^2
h	vane width, mm
n_s	specific speed
n	rotation speed, rpm
u_2	velocity of impeller trailing edge, m/s
v_r	radial velocity, m/s
v_c	circumferential velocity, m/s
ε	energy dissipation, m^2/s^3
ψ	energy loss, $N/(m^2 \cdot s)$

References

1. Shimizu, Y.; Toyosada, K.; Yoshitaka, M.; Sakaue, K. Creation of carbon credits by water saving. *Water* **2012**, *4*, 533–544. [CrossRef]
2. Wong, L.T.; Mui, K.; Lau, C.; Zhou, Y. Pump efficiency of water supply systems in buildings of Hong Kong. *Energy Procedia* **2014**, *61*, 335–338. [CrossRef]
3. Cheng, C.-L. Study of the inter-relationship between water use and energy conservation for a building. *Energy Build.* **2002**, *34*, 261–266. [CrossRef]
4. Plappally, A. Energy requirements for water production, treatment, end use, reclamation, and disposal. *Renew. Sustain. Energy Rev.* **2012**, *16*, 4818–4848. [CrossRef]
5. Cheung, C.; Mui, K.W.; Wong, L.T. Energy efficiency of elevated water supply tanks for high-rise buildings. *Appl. Energy* **2013**, *103*, 685–691. [CrossRef]
6. Volk, M. *Pump Characteristics and Applications*; Taylor&Francis Group CRC Press: Boca Raton, FL, USA, 2013.
7. Zhu, X.; Xie, C.; Jiang, W.; Li, G. Numerical investigation of clocking effect on irreversible energy loss in volute for centrifugal pump with vaned diffuser based on entropy generation method. *Proc. Inst. Mech. Eng. Part C J. Mech. Eng. Sci.* **2023**, *237*, 3430–3443. [CrossRef]
8. Feng, J.; Ge, Z.; Yang, H.; Zhu, G.; Li, C.; Luo, X. Rotating stall characteristics in the vaned diffuser of a centrifugal pump. *Ocean Eng.* **2021**, *229*, 108955. [CrossRef]
9. Li, D.; Zhang, N.; Jiang, J.; Gao, B.; Alubokin, A.A.; Zhou, W.; Shi, J. Numerical investigation on the unsteady vortical structure and pressure pulsations of a centrifugal pump with the vaned diffuser. *Int. J. Heat Fluid Flow* **2022**, *98*, 109050. [CrossRef]
10. Posa, A. LES investigation on the dependence of the flow through a centrifugal pump on the diffuser geometry. *Int. J. Heat Fluid Flow* **2021**, *87*, 108750. [CrossRef]
11. Alubokin, A.A.; Gao, B.; Ning, Z.; Yan, L.; Jiang, J.; Quaye, E.K. Numerical simulation of complex flow structures and pressure fluctuation at rotating stall conditions within a centrifugal pump. *Energy Sci. Eng.* **2022**, *10*, 2146–2169. [CrossRef]
12. Takamine, T.; Watanabe, S. Numerical investigation of radial thrust fluctuation caused by diffuser rotating stall in a centrifugal pump. *J. Phys. Conf. Ser.* **2022**, *2217*, 012031. [CrossRef]
13. Takao, S.; Konno, S.; Ejiri, S.; Miyabe, M. Suppression of Diffuser Rotating Stall in A Centrifugal Pump by Use of Slit Vane. In *Fluids Engineering Division Summer Meeting*; American Society of Mechanical Engineers: New York City, NY, USA, 2021. [CrossRef]
14. Takao, S.; Konno, S.; Ejiri, S.; Miyabe, M. Effect of diffuser vane slit on rotating stall behavior and pump performance in a centrifugal pump. *J. Phys. Conf. Ser.* **2022**, *2217*, 012054. [CrossRef]
15. Vermunt, E.; Bruurs, K.A.J.; Van Der Schoot, M.S.; Van Esch, B.P.M. Part load instability and rotating stall in a multistage low specific speed pump. In *Fluids Engineering Division Summer Meeting*; American Society of Mechanical Engineers: New York City, NY, USA, 2020. [CrossRef]
16. Zeng, Y.; Yao, Z.; Tao, R.; Liu, W.; Xiao, R. Effects of lean mode of blade trailing edge on pressure fluctuation characteristics of a vertical centrifugal pump with vaned diffuser. *J. Fluids Eng.* **2021**, *143*, 111201. [CrossRef]
17. Ye, W.; Geng, C.; Ikuta, A.; Hachinota, S.; Miyagawa, K.; Luo, X. Investigation on the impeller-diffuser interaction on the unstable flow in a mixed-flow pump using a modified partially averaged Navier-Stokes model. *Ocean Eng.* **2021**, *238*, 109756. [CrossRef]
18. Goto, A.; Zangeneh, M. Hydrodynamic design of pump diffuser using inverse design method and CFD. *J. Fluids Eng.* **2002**, *124*, 319–328. [CrossRef]
19. Wu, T.; Wu, D.; Ren, Y.; Song, Y.; Gu, Y.; Mou, J. Multi-objective optimization on diffuser of multistage centrifugal pump base on ANN-GA. *Struct. Multidiscip. Optim.* **2022**, *65*, 182. [CrossRef]
20. Wang, W.; Yuan, S.Q.; Pei, J.; Zhang, J.F. Optimization of the diffuser in a centrifugal pump by combining response surface method with multi-island genetic algorithm. *Proc. Inst. Mech. Eng. Part E J. Process Mech. Eng.* **2017**, *231*, 191–201. [CrossRef]
21. Gülich, J.F. *Centrifugal Pumps*; Springer: Heidelberg, Germany, 2014.

22. Cubas, J.; Stel, H.; Ofuchi, E.M.; Neto, M.A.M.; Morales, R.E. Visualization of two-phase gas-liquid flow in a radial centrifugal pump with a vaned diffuser. *J. Pet. Sci. Eng.* **2020**, *187*, 106848. [CrossRef]
23. Shim, H.-S.; Kim, S.-H.; Kim, K.-Y. Analysis and optimization of staggered partial diffuser vanes in a centrifugal pump. *J. Fluids Eng.* **2020**, *142*, 051207. [CrossRef]
24. Zhu, X.; Li, G.; Jiang, W.; Fu, L. Experimental and numerical investigation on application of half vane diffusers for centrifugal pump. *Int. Commun. Heat Mass Transf.* **2016**, *79*, 114–127. [CrossRef]
25. Fu, L.; Zhu, X.; Jiang, W.; Li, G. Numerical investigation on influence of diffuser vane height of centrifugal pump. *Int. Commun. Heat Mass Transf.* **2017**, *82*, 114–124. [CrossRef]
26. Moffat, R.J. Describing the uncertainties in experimental results. *Exp. Therm. Fluid Sci.* **1988**, *1*, 3–17. [CrossRef]
27. Li, D.; Wang, H.; Qin, Y.; Han, L.; Wei, X.; Qin, D. Entropy production analysis of hysteresis characteristic of a pump-turbine model. *Energy Convers. Manag.* **2017**, *149*, 175–191. [CrossRef]
28. Li, X.; Jiang, Z.; Zhu, Z.; Si, Q.; Li, Y. Entropy generation analysis for the cavitating head-drop characteristic of a centrifugal pump. *Proc. Inst. Mech. Eng. Part E J. Process Mech. Eng.* **2018**, *232*, 4637–4646. [CrossRef]